ACS central science

Research Article

Cite This: ACS Cent. Sci. 2019, 5, 1857−1865

http://pubs.acs.org/journal/acscii

Light-Enhanced Ion Migration in Two-Dimensional Perovskite Single Crystals Revealed in Carbon Nanotubes/Two-Dimensional Perovskite Heterostructure and Its Photomemory Application

Yu-Tao Li,[†,#] Li Ding,[‡,#] Jun-Ze Li,[∥,#] Jun Kang,[§] De-Hui Li,[∥] Li Ren,[‡] Zhen-Yi Ju,[†] Meng-Xing Sun,[†] Jia-Qi Ma,[∥] Ye Tian,[†] Guang-Yang Gou,[†] Dan Xie,[†] He Tian,[†] Yi Yang,[†] Lin-Wang Wang,[*,§] Lian-Mao Peng,[*,‡] and Tian-Ling Ren[*,†]

[†]Institute of Microelectronics, Beijing National Research Center for Information Science and Technology (BNRist), Tsinghua University, Beijing 100084, China

[‡]Key Laboratory for the Physics and Chemistry of Nanodevices and Department of Electronics, Key Laboratory for the Physics and Chemistry of Nanodevices and College of Chemistry and Molecular Engineering, Peking University, Beijing 100871, China

[§]Material Science Division, Lawrence Berkeley National Laboratory, Berkeley, California, United States

[∥]School of Optical and Electronic Information, Huazhong University of Science and Technology, Wuhan 430074, China

Supporting Information

ABSTRACT: Two-dimensional (2D) hybrid perovskite sandwiched between two long-chain organic layers is an emerging class of low-cost semiconductor materials with unique optical properties and improved moisture stability. Unlike conventional semiconductors, ion migration in perovskite is a unique phenomenon possibly responsible for long carrier lifetime, current−voltage hysteresis, and low-frequency giant dielectric response. While there are many studies of ion migration in bulk hybrid perovskite, not much is known for its 2D counterparts, especially for ion migration induced by light excitation. Here, we construct an exfoliated 2D perovskite/carbon nanotube (CNT) heterostructure field effect transistor (FET), not only to demonstrate its potential in photomemory applications, but also to study the light induced ion migration mechanisms. We show that the FET $I-V$ characteristic curve can be regulated by light and shows two opposite trends under different CNT oxygen doping conditions. Our temperature-dependent study indicates that the change in the $I-V$ curve is probably caused by ion redistribution in the 2D hybrid perovskite. The first principle calculation shows the reduction of the migration barrier of I vacancy under light excitation. The device simulation shows that the increase of 2D hybrid perovskite dielectric constant (enabled by the increased ion migration) can change the $I-V$ curve in the trends observed experimentally. Finally, the so synthesized FET shows the multilevel photomemory function. Our work shows that not only we could understand the unique ion migration behavior in 2D hybrid perovskite, it might also be used for many future memory function related applications not realizable in traditional semiconductors.

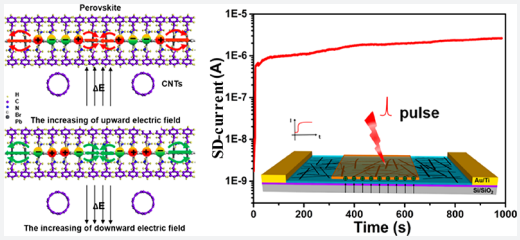

INTRODUCTION

Halide perovskites are an attractive photoactive material with high light absorption coefficients,[1] intense photoluminescence,[2] slow rates of nonradiative charge recombination[3,4] and a low-cost preparation process,[5,6] and have been successfully applied to various lab-scale optoelectronic devices such as solar cells,[1,7,8] light emitting diodes (LEDs),[9−11] and lasers.[9,12] Recently, two-dimensional (2D) layered perovskites with a general formula of $(L)_2(SMX_3)_{n+1}MX_4$, where L, S, M, and X represent long-chain organic cations, short-chain organic cations, divalent metal cation, and halide, respectively, and n is the number of SMX_3 monolayer sheets sandwiched between two long-chain organic layers, have emerged as an intensely studied quantum-well structure[13] with unique optical properties[14,15] and improved moisture stabilities.[16] Despite this progress, significant challenges remain regarding both the stability of the 2D layered perovskites and how to use their unique properties in applications.[16−19] Compared with conventional photoelectric material, halide perovskite material is characterized by a mixed conducting behavior that possesses both electronic and ionic conductivity.[20−25] Ionic transport has been suggested to be an important factor contributing to unusual behavior such as poor stability,[26] current−voltage hysteresis,[27−29] and a low-frequency giant dielectric response[30,31] in a perovskite-based optical device. Therefore, the study of ion migration in perovskite is of great value to understand its underlying physics and application potential. While there are many ion migration studies in three-

Received: August 20, 2019
Published: October 21, 2019

DOI: 10.1021/acscentsci.9b00839
ACS Cent. Sci. 2019, 5, 1857−1865

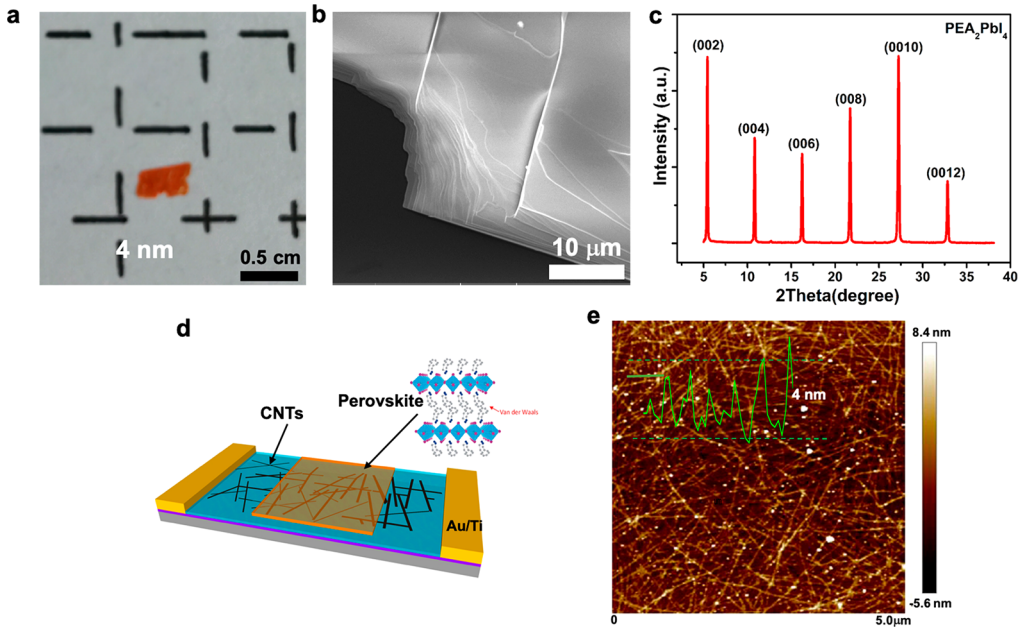

Figure 1. Material characterization and device schematic of the perovskite/CNTs heterojunction. (a) Photo of an as-grown $(PEA)_2PbI_4$ single crystal. (b) SEM image of an as-grown $(PEA)_2PbI_4$ single crystal. (c) XRD pattern of an as-grown $(PEA)_2PbI_4$ single crystal. (d) Device schematic diagram of a perovskite/CNTs heterojunction transistor. (e) AFM image of as-grown CNTs, and the green lines show the profile of CNTs network.

dimensional (3D) halide perovskites, the related studies in 2D perovskites are still scarce.

The photoelectric device is another application area for 2D layered perovskites with great potential.[32−34] It has been reported that continuous light illumination can cause the unstable performance of the 2D layered perovskites.[35] However, a deeper understanding of such behavior might allow us to turn around the situation and make such unique properties as a merit in other applications, especially the ones related to memory functions. In recent years, searching materials for nonvolatile memory applications, memristor or photomemory devices, have attracted major attention. The adequate materials often require ion migration in order to reach nonvolatile metastable states. In this regard, halide perovskite could be a good candidate due to its great tendency in ion migration, especially under external stimulations like light. However, only a few experiments have investigated the effect of light on halide perovskite and they mainly focus on the study of bulk 3D perovskite single crystals.[36−39] For example, Zhao et al.[36] quantitatively demonstrated light-enhanced ionic transport in $CH_3NH_3PbI_3$ over a wide temperature range and revealed a reduction in ionic transport activation energy under illumination. Tsai et al.[37] also reported that continuous light illumination leads to a uniform lattice expansion in hybrid perovskite thin films. In contrast, the effect of light-induced ion migration in 2D layered perovskite remains elusive. One of the main reason is that the organic chain coating of the layered perovskite material makes it difficult to measure the current.[14,15,40,41] Thus, in order to study the light induced effect, it is useful to design systems where no direct charge current measurement from the 2D perovskite is necessary. Such a study will also help us to develop novel applications based on the light-induced phenomenon in 2D perovskite systems. Given the more prominent role of the surface organic ligand, the light induced ion migration effect in 2D perovskite can be rather different from its 3D counterparts.

In this work, we investigate the light-enhanced ion migration in 2D perovskite single crystals using a CNTs/2D perovskite heterostructure field-effect transistor (FET). Since the conductivity of single-wall semiconductor CNTs is sensitive to its environmental electrostatic potentials, CNTs can be used as a probe to monitor the ion redistribution within a 2D perovskite sheet under light excitation. The influence of light on 2D perovskite is converted into the change of the device I−V curve characteristic of the CNTs/2D perovskite FET. Besides, ab initio calculations are used together with the device level simulations to understand the influence of ion migration to the FET characteristics. Finally, the photomemory effect of CNTs/2D perovskite heterostructure FET was demonstrated, and the optical and electrical multivalued two-phase photomemory functionality was achieved.

MATERIAL CHARACTERIZATION AND DEVICE FABRICATION

High-quality, millimeter-sized 2D $(PEA)_2PbI_4$ perovskite single crystals (PEA: phenethylammonium) were synthesized using an antisolvent vapor crystallization method[15] as shown in Figure 1a. Through a tape-based mechanically exfoliated method, the 2D perovskite can be exfoliated into thin layers, and the 2D layered morphology of perovskite can be clearly seen through a scanning electron microscope (SEM) image (Figure 1b). The X-ray diffraction (XRD) patterns of as-grown 2D perovskite single crystals are investigated in Figure 1c, which confirms the phase purity. The layered crystal structure and the weak van der Waals forces between the organic molecules in perovskite layers (inset in Figure 1d) allow for the exfoliation of 2D perovskite single crystals into ultrathin sheets, which is convenient for the manufacture of subsequent devices.

In order to investigate the light-induced ions migration in 2D perovskite single crystals, we designed a CNTs/2D

DOI: 10.1021/acscentsci.9b00839
ACS Cent. Sci. 2019, 5, 1857−1865

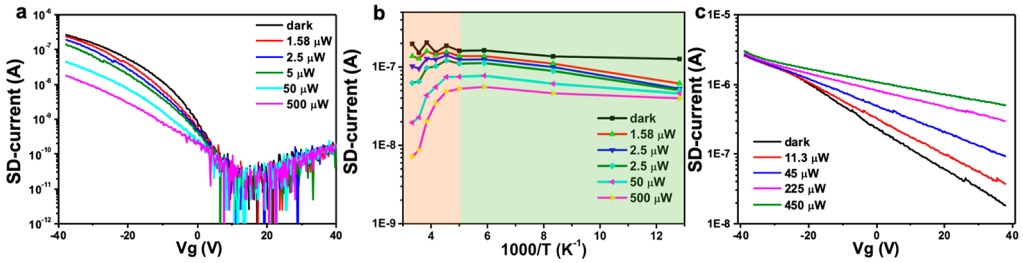

Figure 2. SD-current of perovskite/CNTs heterojunction. (a) SD-current of perovskite/CNTs heterojunction in a vacuum chamber. (b) The SD-current varies with temperature under a gate voltage of −30 V. (c) SD-current of perovskite/CNTs heterojunction with an oxygen doping condition.

perovskite heterostructure. Figure 1d schematically shows the structure of the device. A thin film of wafer-scale semiconductor CNTs was first deposited on a highly doped Si substrate with a 500 nm oxide layer (see Methods section for more details). The 80 nm Pd electrode pads with a 20 μm-length channel were made by electron beam lithography and electron beam evaporation. After that, a 2D perovskite thin crystal sheet is exfoliated and transferred on the CNTs channel based on well-known 2D dry transfer methods,[42] forming an atomic smooth interface via the van der Waals force between perovskite and CNTs. It is worth mentioning that the 2D perovskite sheet only covers the center of CNTs and does not contact pads at both ends (schematic diagram of Figure 1d). Thus, the current between source and drain electrodes is completely derived through CNTs, and there is no charge current generated from the 2D perovskite. Figure 1e shows the network structure of CNTs thin films, which indicates that the interface between CNTs and perovskite can be divided into suspended and contact parts (the Raman results in the Figure S1b represent the s-SWCNT with an average diameter of 1.57 nm[43,44]). It is worth noting that the special structure of the interface layer is the key to the parallel nonequilibrium distribution of ions and charges under the back-gate electric field, thus forming the photogating effect under light illumination.

PHOTOGATING EFFECT IN CNTs/TWO-DIMENSIONAL PEROVSKITE HETEROSTRUCTURE

Before the test of photoresponse of the CNTs/2D perovskite heterostructure, the electrical characteristics of pure CNTs FET were measured first. Shown in Figure S2, the transfer curve of pure CNTs FET shows no response to light of 470 nm. Then, the photoresponse of the CNTs/2D perovskite heterostructure was tested under constant steady state light illuminations (Figure 2a). The device was placed in a vacuum chamber, and the gate voltage was scanned from −40 V to +40 V, while the source-drain bias is −1 V. At the same time, a light of 470 nm with tunable intensity will illuminate on the device in parallel. As can be seen, with the increase of light intensity (dark to 500 μW), the source/drain current reduces, showing a negative photogating effect. This again indicates that there is no photocurrent injecting to CNT from the 2D perovskite. When the gate voltage was −40 V, the percentage of SD-current drop was the largest, reaching 94% (from 285 to 16.7 nA).

LIGHT-ENHANCED IONS MIGRATION IN TWO-DIMENSIONAL PEROVSKITE

As will be discussed further in later sections, we believe the negative photogating effect is due to the dielectric screening exerted from the 2D perovskite onto the CNT. The light illumination has increased the dielectric constant of the 2D perovskite (or the coated organic chain), which can effectively increase the screen effect of the gate voltage toward a charge neutral state. In this case, the neutral state (defined in the following parts) is probably about V_g = 5 V. Thus, in Figure 2a, under illumination, for a given negative V_g, the after screened effective V_g will be closer to zero, which will reduce the current (according to the dark curve in Figure 2a). Our device simulation to be discussed later will confirm this picture.

There are however two possible causes for the increased dielectric screening of the 2D perovskite under light illuminations. One is the photo-generated electron−hole free carrier.[36] However, such carrier-generated screening should be transient, disappearing with the light, and there should be no lasting memory effect. As will be shown in Figure 4b, when the device is excited with a one-second laser pulse, it will have a long-lasting effect for the source-drain (SD) current after the laser light pulse. This indicates the prominent role of ion migration. Such ion migration will sensitively depend on the temperature. To test this, we have measured the temperature dependence of the SD-current under different light illuminations, while the gate voltage is fixed at −30 V. The results are shown in Figure 2b.

As shown in Figure 2b, the SD-current first increases (red region) and then decreases (green region) with the decrease of temperature, and the maximum value is obtained at about 200 K. The biggest photogating effect happens at high illuminations and high temperature. This is due to the overcoming of the ion diffusion barrier. At low enough temperature (green region in Figure 2b), however, the ion diffusion is suppressed. In this region (green in Figure 2b), the SD-current decreases with decreasing temperature because of depressed thermionic effect carrier transport[45] as in the Schottky-Barrier contact (demonstrated in Figure S5) between CNT and SD metals (see Methods). Figure S3 shows the change in SD-current in pure CNTs without 2D perovskite with different temperatures, which is small, but the current decreases with temperature, in the same trend as in the green region of Figure 2b. Furthermore, in Figure 2b, we also see a decrease of the SD-current when the illumination intensity increases at a given low-temperature point (in the green region). This can be attributed to the photo-generated electron−hole carrier screening effect inside 2D perovskite, which does not depend on the temperature. Finally, one additional device was

DOI: 10.1021/acscentsci.9b00839
ACS Cent. Sci. 2019, 5, 1857−1865

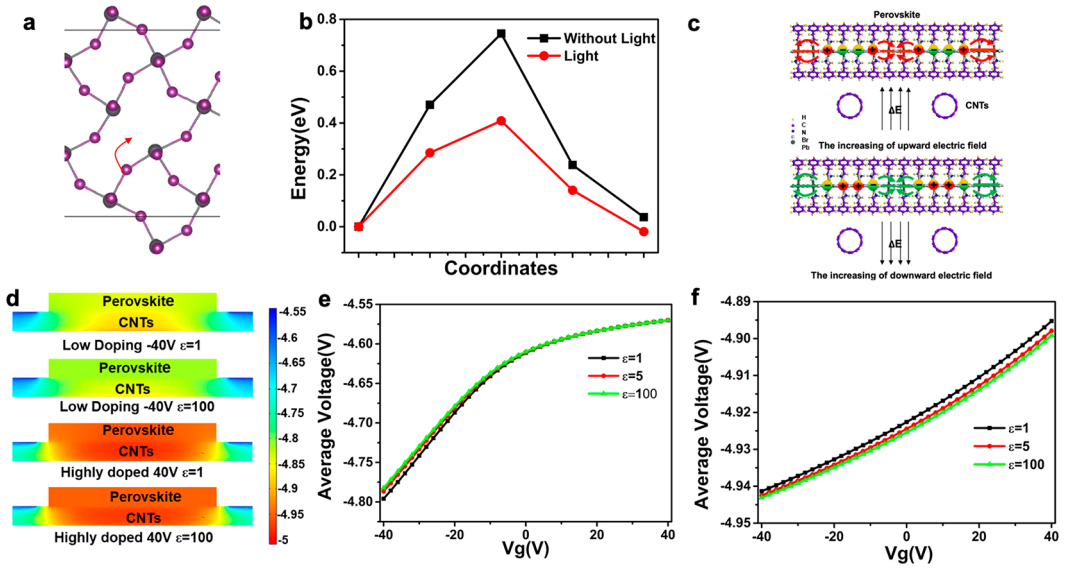

Figure 3. Simulation of the perovskite/CNTs heterojunction. (a) Ion immigration path of NEB calculation. (b) The migration barrier of perovskite ions in original and excited states. (c) Schematic diagram of in-plane ion migration of perovskite under electric field. ΔE represents the change of back-gate electric field and the arrows in the perovskite represent the moving directions of the charges inside it. (d) Potential distribution of perovskite/CNTs heterojunction at different dielectric constants and doping concentrations. The average potential distribution of perovskite/CNTs heterojunction under different dielectric constants in (e) low oxygen doping condition and (f) high oxygen doping condition.

fabricated to verify the repeatability of the above phenomenon (Figure S4), which demonstrated the same trends.

P-TYPE DOPING OF CNTs CHANNELS FOR PHOTOGATING EFFECT ADJUSTMENT IN CNTs/2D PEROVSKITE HETEROSTRUCTURE

It is known that water and oxygen molecules would be adsorbed[46−48] in channels of back-gated CNT transistors when exposed in an ambient environment. This might induce p-type doping and SD-current improvement. Shown in Figure 2c, when the device was tested under the atmospheric environment, the SD-current is significantly larger due to the p-type doping on CNTs, and the threshold voltage was significantly moved to the positive half axis. Interestingly, the SD-current of the device shows an opposite trend under this test conditions. This change of SD-current trend is surprising. One possible reason is that the unscreened charge neutral point has been shifted toward the negative gate voltage (about −35 V). This unscreened neutral point is defined as the gate voltage point where there is no lateral electric field inside the 2D perovskite near the CNT. Thus, if light illumination can increase the dielectric screening, it will bring the system toward this neutral voltage point, which is at the left-hand side of Figure 2c, and thus will increase the SD-current as shown in Figure 2c. The detailed effect of the increasing dielectric screening can be obtained through actual device simulation with different doping on CNT and gate bias, as we will show in next section.

SIMULATION ON CNTs/2D PEROVSKITE HETEROSTRUCTURE

To understand why light illumination induced ion migrations, we have carried out ab initio calculations. It has been shown that halogen vacancy migration is dominant in hybrid perovskite.[49] Therefore, we studied the migration barrier of I vacancy from first-principles calculations (see Methods section for more information). Here neutral vacancy (V_I) and charged vacancy (V_I^+) are considered. V_I creates a defect state occupied by one electron inside the band gap. With light excitation, the electron can be excited into a conduction band, and the defect becomes positively charged. Therefore, the cases for V_I and V_I^+ can correspond to dark and light excitation conditions, respectively. As for the ion migration path, the total energy of the out-of-plane defect is 0.4 eV higher than that of the in-plane defect. Thus, the in-plane defect is more stable and should be considered. Figure 3a shows the ion migration path (the red arrow) during the calculation, and Figure 3b demonstrates that the ion migration barrier decreased from 0.74 eV in the case of V_I to 0.41 eV in the case of V_I^+ under one photoexcitation. This shows the significant reduction of the diffusion barrier under light illumination. The increased ability for ion diffusion effectively increases the dielectric constant in the 2D perovskite.[50,51] The DFT calculation does show it is feasible that such significant reduction of the ion migration barrier is possible during light illuminations. Besides, during the calculation, it is found that the Pb−Pb distance around the V_I is different when the charge state changes. In the neutral case, the Pb−Pb distance is 5.60 Å, whereas in the +1 charged case the distance is 6.28 Å. This indicates a stronger Pb−Pb interaction in the neutral case, since the extra electron can induce some covalent-bond-like interaction between them. The I migration thus involves a process of breaking the Pb−Pb covalent interaction, which requires a relatively higher barrier energy. On the other hand, in the charged case there is no such covalent interaction, leading to a smaller barrier energy. That may be a possible reason for the reduction of the migration barrier.

Before device level simulations, it will be helpful to have a qualitative picture about the screening effect. Note that, if instead of having a nanotube, we have a planar active layer for SD current, the 2D perovskite will have no screening effect on the active layer because it cannot exert a perpendicular electric field outside the 2D perovskite layer. Thus, the true screening effect comes from the finite lateral size of the CNT, and the

DOI: 10.1021/acscentsci.9b00839
ACS Cent. Sci. 2019, 5, 1857−1865

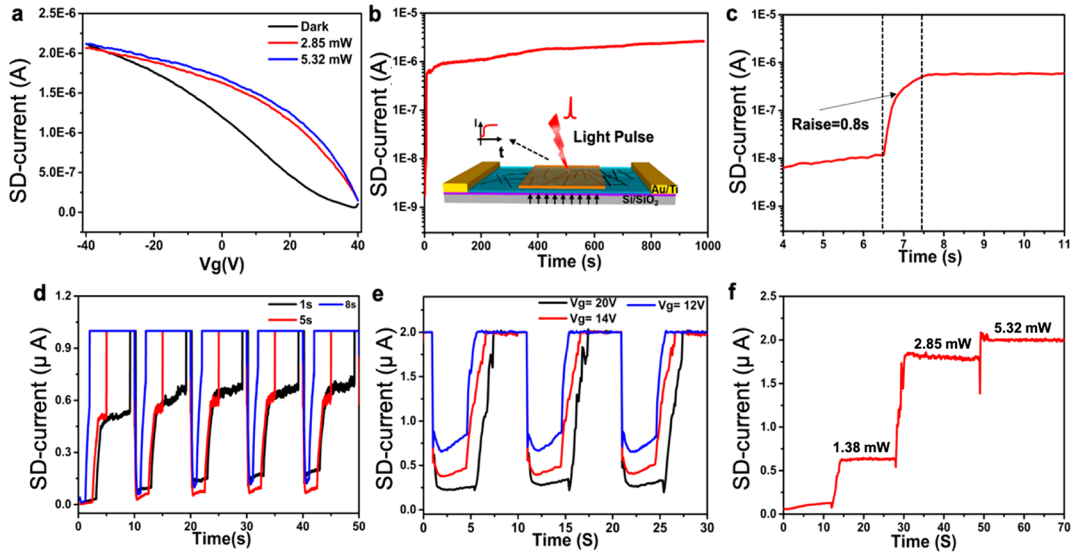

Figure 4. Photomemory based on perovskite/CNTs heterojunction. (a) Proper transfer curve of perovskite/CNTs heterojunction. (b) Photomemory test results and schematic diagram. (c) Enlarged time-threshold graph of the photomemory response. (d) Erasable test of photomemory device under different erasing time. (e) Electrical multivalue storage with different high resistance states. (f) Optical multivalue storage with different low resistance states.

migration of the charge in the lateral direction with the 2D perovskite layer as schematically illustrated in Figure 3c.

We then perform comsole device simulation using the finite element method. Such simulation can be used to calculate the average potential on the CNT as a function of the gate voltage and the 2D perovskite dielectric constant. One can also introduce p-doping in the CNT to exchange the band alignment between CNT and the gate. In the simulation, the potential change on the CNT under the scanning gate voltage is observed. The 2D perovskite covers the CNT, affecting the potential of the device. CNTs under different doping conditions are calculated to confirm the experimental results. As shown in Figure 3d, the fastest changing area of the voltage is different for different doping, which is consistent with the change of average voltage on the CNT (see Supporting Information for more details about device simulation). Figure S7 shows the schematic diagram of the simulation model, and Figure 3c reflects the conceptual schematic of the material interface. Same for the real situation, CNTs are represented by a cylindrical structure, and the interface area with perovskite can be divided into two parts (suspended and contact parts), as mentioned above. Thus, this cylindrical structure causes the in-plane redistribution of the internal nonequilibrium carriers and ions, which results in the photogating effect. The extra photogating effect of the perovskite layer can cause the redistribution of the potential in the nanotube, thus changing the nanotube electric transport. Generally, the increasing of the downward electric field (positive bias) will cause the accumulation of positive charges in the perovskite above CNTs to inhibit the increasing of CNTs current, and the increasing of an upward electric field will cause the opposite effect (Figure 3c), which is consistent with Figure 2a,c. Figure 3e shows that, in the absent of doping, the dielectric screening of the 2D perovskite will indeed bring the effective voltage on the CNT toward a less negative value, which reduces the SD-current as shown in Figure 2a. On the contrary, as shown in Figure 3f, in the case of p-type doped CNT, the screening will make the potential on CNT more negative, thus increasing the SD-current, as shown in Figure 2c. The influence of p-type doping on the perovskite neutral point is shown in Figure S8, in which the electric field intensity at the interface between CNTs and perovskite varies inversely with the gate voltage under different doping conditions and confirms that the neutral point voltage is obviously moved to the negative half axis under p-type doping and matches the previous hypothesis well. This explains qualitatively the two opposite trends shown in Figure 2a,c. However, we do notice that the amplitudes shown in Figure 3e,f seem much smaller than the photogating effect shown in Figure 2, although the qualitative trend is the same. One possibility is that, in reality, the critical point determining the current is not in the CNT themselves, but is at their junction points as shown in Figure 1d. Those junction points are 0D point structures, which might have much stronger lateral screening effects. Nevertheless, the trend will be the same as shown above.

PHOTOMEMORY DEMONSTRATION

Through the above studies by the combination of experiment and calculation, the light-enhanced ion migration effect in 2D layered perovskite was revealed. As an application demonstration, it is expected to be utilized to fabricate photomemory devices. In short, light will change the ion migration barrier in 2D perovskite. Under strong light conditions, ions are more likely to move to the interface under the influence of the external electronic field, thus weakening the influence of the external field on the material system. In a dark environment, ions are more likely to be trapped in the 2D perovskite because of the high migration barrier. The details of the photomemory process are shown in Figure S11 and can be divided into four states, which are carefully discussed in the Supporting Information. According to this effect, we can select appropriate light intensity and external electric field conditions and achieve optical storage application through this CNTs/2D perovskite heterostructure FET.

Shown in the Figure 4a, due to the photogating effect of 2D layered perovskite, the transfer curve of CNTs/2D layered perovskite hetrostructure FET will be raised when 470 nm

DOI: 10.1021/acscentsci.9b00839
ACS Cent. Sci. 2019, 5, 1857−1865

light with 2.85 mW intensity is irradiated on the device (red line). Besides, when the light intensity is further increased (5.32 mW in Figure 4a), the transfer curve is further increased but almost overlapped, indicating that the photogating effect of perovskite under this light intensity is close to saturation. In addition, the opening window by light was the largest when the backgate voltage was 20 V by proper adjustment. Therefore, the illumination intensity of 2.85 mW and the backgate voltage of 20 V were chosen to subsequently test the optical memory characteristics. Figure 4b shows the photoelectric response of the device in the time domain. When a beam of 1 s light pulse was irradiated on the device, the photoelectric current of the device increased rapidly (with on/off radio ∼100). Besides, even if the light disappears, the SD-current of the device can remain at a high value for more than 1000 s, without showing a downward trend. This is because ions migrated under light conditions are trapped in a quasi-steady state in dark environment. Figure 4c shows an enlarged view of the rising curve of the SD-current, which demonstrates that the optical response of the device is very fast with the rising time about 0.8 s. To verify the erasable properties of photomemory devices, we reversed the back-gate voltage (from +20 V to −20 V) to restore 2D perovskite to its initial state. The device was tested to verify the erasing repeatability of a photomemory device with a current compliance of 1 μA during the measurement. It is found that the device can return to the same initial state horizontally (on/off ratio of ∼120 in Figure 4d) at different erasure times (1 s, 5 s, 8 s) with good stability. To make the testing process clearer, Figure S12 shows the enlarged time sequence corresponding to back gate voltage, pulse light source, and SD-current. Finally, by adjusting the back-gate voltage or illumination intensity under a quasi-steady state, we realized the multivalued two-phase storage with good repeatability in a new sample (testing details are shown in the Supporting Information). Among them, the back-gate voltage realizes electrical multivalue storage (Figure 4e) by changing the semiconductor property of the CNTs probe, while the light intensity realizes optical multivalue storage (Figure 4f) by changing the migration barrier of ions. This study of optical storage applications opens the way for new applications in the perovskite field.

CONCLUSION

In summary, we have studied the light-enhanced ions migration in 2D perovskite single crystals through CNTs/2D perovskite heterostructure. Furthermore, we found that light can influence the transfer characteristic curve of in this heterostructure by a photogating effect and shows two change tendencies under different oxygen doping conditions. On the basis of the temperature-dependent measurement, light-enhanced ion migration in 2D perovskite was confirmed. First principle combined with finite element analysis is performed to verify that the transfer characteristic is relative to a tunable ion migration barrier under various light intensities. Finally, by designing appropriate test conditions, CNTs/2D perovskite heterostructure realizes the function of photomemory with a multivalue, erasable two-phase performance. This study not only provides experimental and theoretical support for light-enhanced ion migration in 2D perovskite, but also demonstrates the potential of 2D perovskite as a promising candidate material for photomemory application.

METHODS

In this section, no unexpected or unusually high safety hazards were encountered.

Material Preparation. *Synthesis of $(PEA)_2PbI_4$.* PEAI was synthesized by mixing phenethylamine (Sigma-Aldrich) with hydriodic acid (HI Sigma-Aldrich) in a 1:1 molar ratio at 0 °C with constant stirring for 4 h. The solvent was then evaporated at 60 °C and washed by cold diethyl for several times. At last, resultant was dried at 70 °C for 12 h. For synthesis of $(PEA)_2PbI_4$ perovskite, 0.5 g of lead oxide powder (PbO Sigma-Aldrich) was dissolved in a mixture solution of 3 mL of HI and 0.5 mL of hypophosphorous acid (H_3PO_2 Sigma-Aldrich). Then the solution was heated to 140 °C with stirring. After that, 2.5 mmol of PEAI solution was added into the solution. At last, the stirring was stopped, and the solution was naturally cooled down to room temperature for crystallization.

Preparation of CNTs Film. Arc-discharged CNTs were purchased from Carbon Solutions Inc., and the dispersants (poly[9-(1-octylonoyl)-9*H*-carbazole-2, 7-diyl (PCz)]) were synthesized by Suzuki polycondensation.[47] First, CNTs and PCz were added into toluene to forma solution, and then the solution was dispersed with a top-tip dispergator (Sonics VC700) at 300 W for 30 min. Second, the dispersed solution was centrifuged for 0.5 h at 50000*g* to remove most of the metallic CNTs and insoluble materials. The upper 90% of the supernatant was collected and centrifuged for a second centrifugation for 2 h at 50000*g*. Finally, upper 90% of the supernatant was collected as semiconducting single-walled CNTs (s-SWCNTs) for the fabrication of thin film with a dip-coating method. The s-SWCNT solution was diluted several times with the toluene for the preparation of CNT film. SiO_2/Si substrates with a small size (smaller than 5 cm × 5 cm) were immersed in the diluted solution for 3 days, and then picked up and purged by high-purity nitrogen. The substrate with CNT film was first immersed in toluene for 10 min and then purged with high-purity nitrogen. The air in the tube furnace (Thermo Scientific Linderg/Blue M MoldathERM 1100 °C) was blown away using 1000 sccm argon and the substrate covered by the CNT film was put in the tube furnace to be annealed for 3 h. The detailed annealing temperature was set to 600 °C, and the argon and hydrogen flow rates were 300 and 50 sccm, respectively. After the annealing process, we immediately repeatedly rinsed the substrate with CNT film in isopropanol (IPA).

Device Fabrication and Characterization. In general, electron beam lithography (EBL) is the most important nanofabrication process for patterning. Before each EBL process, poly(methyl methacrylate) (PMMA) was spin-coated as positive resist (in most cases, 4000 rpm followed by a 3 min 170 °C bake). First, Ti/Au films (10 nm/40 nm) were patterned by EBL and deposited as standard alignment marks. Second, CNT-film active regions were patterned by an EBL process followed by an inductively couple plasma (ICP) etching. Third, p-FET contacts were formed by an EBL process and the deposition of 80 nm Pd films through electron beam evaporation (EBE) followed with a standard lift-off process to make planar back gate field effect transistor with 5 μm × 20 μm channel. And then, a PDMS stamp was used to pick up the 2D perovskite flakes and transfer the 2D perovskite flakes onto CNTs to form a CNTs/2D perovskite heterostructure. A photogating effect test of the FET was carried out using a Keithley 4200A parameter analyzer in a vacuum

DOI: 10.1021/acscentsci.9b00839
ACS Cent. Sci. 2019, 5, 1857−1865

chamber, while a photomemory test was performed using an Agilent B1500A in a Lakeshore cryogenic probe station.

Methods of Simulation. *Calculation Details for the First Principle Study.* Density functional calculations were performed using the Pwmat code.[52,53] The norm-conserving pseudopotentials[54] and the PBE functional[55] were adopted. The planewave cutoff energy was 40 Ry. Structure relaxation was stopped when the force on each atom was less than 0.02 eV/Å. A 2 × 2 × 1 supercell was used to simulate an isolated I vacancy, and the vacuum layer was larger than 10 Å. The Brillioun zone is sampled by the Gamma point. Migration barrier was calculated by the nudged elastic band (NEB) method.[49]

Calculation Details for Finite Element Simulation. The structure of CNT is an elliptic cylinder of 0.6 nm semimajor axis, 0.5 nm semiminor axis, and 10 nm length. Perovskites was set as a 6 × 2 × 1 nm cuboid. The contact area of CNT and perovskites is a rectangle of 6 × 0.1 nm. The size of metal contact area of CNT is 1 × 0.1 nm. In the finite element simulation, the semiconductor module was used to calculate the potential of the device. The metal electrodes were set as Schottky contact with CNT, with a 4.55 eV work function. The back-gate electrode was scanned from −40 to 40 V. And the thickness of the insulator was set as 800 nm. Two different doped concentrations of CNT were considered in the simulation. The low-doped concentration was 1.0×10^{17} cm^{-3}, and the high-doped concentration was 5.0×10^{18} cm^{-3}. The dielectric constant of perovskites varied between 1 and 100. The potential distribution of the device and the average potential of CNT were calculated.

■ ASSOCIATED CONTENT

Supporting Information

The Supporting Information is available free of charge on the ACS Publications website at DOI: 10.1021/acscentsci.9b00839.

Additional figures and data, experimental procedures, simulation details and analytical characterization of CNTs/2D Perovskite heterostructure (PDF)

■ AUTHOR INFORMATION

Corresponding Authors

*(T.-L.R.) E-mail: RenTL@tsinghua.edu.cn.
*(L.-M.P.) E-mail: lmpeng@pku.edu.cn.
*(L.-W.W.) E-mail: lwwang@lbl.gov.

ORCID

Yu-Tao Li: 0000-0002-0665-0683
Jun-Ze Li: 0000-0001-8837-5349
Jun Kang: 0000-0003-4788-0028
De-Hui Li: 0000-0002-5945-220X
Ye Tian: 0000-0002-3278-1126
Guang-Yang Gou: 0000-0002-1174-203X
Dan Xie: 0000-0001-9521-9774
He Tian: 0000-0001-7328-2182

Author Contributions

#Y. T. L., L. D. and J. Z. L. contributed equally to this work.

Notes

The authors declare no competing financial interest.

■ ACKNOWLEDGMENTS

This work was supported by the National Key R&D Program (2016YFA0200400), National Natural Science Foundation (61434001, 61574083, 61874065, 51861145202), and National Basic Research Program (2015CB352101) of China. The authors are also thankful for the support of the Research Fund from Beijing Innovation Center for Future Chip, Beijing Natural Science Foundation (4184091), and Shenzhen Science and Technology Program (JCYJ20150831192224146). J. Kang and L.W. Wang were supported by the Office of Science, the Office of Basic Energy Sciences (BES), Materials Sciences and Engineering (MSE) Division of the U.S. Department of Energy (DOE) under Contract No. DE-AC02-05CH11231 under the Organic/inorganic nanocomposite program (KC3104).

■ REFERENCES

(1) Lee, M. M.; Teuscher, J.; Miyasaka, T.; Murakami, T. N.; Snaith, H. J. Efficient hybrid solar cells based on meso-superstructured organometal halide perovskites. *Science* **2012**, *338* (6107), 643.

(2) Jang, D. M.; Park, K.; Kim, D. H.; Park, J.; Shojaei, F.; Kang, H. S.; Ahn, J.-P.; Lee, J. W.; Song, J. K. Reversible halide exchange reaction of organometal trihalide perovskite colloidal nanocrystals for full-range band gap tuning. *Nano Lett.* **2015**, *15* (8), 5191.

(3) Stranks, S. D.; Eperon, G. E.; Grancini, G.; Menelaou, C.; Alcocer, M. J.; Leijtens, T.; Herz, L. M.; Petrozza, A.; Snaith, H. J. Electron-hole diffusion lengths exceeding 1 micrometer in an organometal trihalide perovskite absorber. *Science* **2013**, *342* (6156), 341.

(4) Yang, Y.; Yan, Y.; Yang, M.; Choi, S.; Zhu, K.; Luther, J. M.; Beard, M. C. Low surface recombination velocity in solution-grown $CH_3NH_3PbBr_3$ perovskite single crystal. *Nat. Commun.* **2015**, *6*, 7961.

(5) Liu, D.; Kelly, T. L. Perovskite solar cells with a planar heterojunction structure prepared using room-temperature solution processing techniques. *Nat. Photonics* **2014**, *8* (2), 133.

(6) Mao, Y.; Banerjee, S.; Wong, S. S. Large-scale synthesis of single-crystalline perovskite nanostructures. *J. Am. Chem. Soc.* **2003**, *125* (51), 15718.

(7) Burschka, J.; Pellet, N.; Moon, S.-J.; Humphry-Baker, R.; Gao, P.; Nazeeruddin, M. K.; Grätzel, M. Sequential deposition as a route to high-performance perovskite-sensitized solar cells. *Nature* **2013**, *499* (7458), 316.

(8) Jeon, N. J.; Noh, J. H.; Kim, Y. C.; Yang, W. S.; Ryu, S.; Seok, S. I. Solvent engineering for high-performance inorganic−organic hybrid perovskite solar cells. *Nat. Mater.* **2014**, *13* (9), 897.

(9) Veldhuis, S. A.; Boix, P. P.; Yantara, N.; Li, M.; Sum, T. C.; Mathews, N.; Mhaisalkar, S. G. Perovskite materials for light-emitting diodes and lasers. *Adv. Mater.* **2016**, *28* (32), 6804.

(10) Xiao, Z.; Kerner, R. A.; Zhao, L.; Tran, N. L.; Lee, K. M.; Koh, T.-W.; Scholes, G. D.; Rand, B. P. Efficient perovskite light-emitting diodes featuring nanometre-sized crystallites. *Nat. Photonics* **2017**, *11* (2), 108.

(11) Zhao, L.; Yeh, Y.-W.; Tran, N. L.; Wu, F.; Xiao, Z.; Kerner, R. A.; Lin, Y. L.; Scholes, G. D.; Yao, N.; Rand, B. P. In situ preparation of metal halide perovskite nanocrystal thin films for improved light-emitting devices. *ACS Nano* **2017**, *11* (4), 3957.

(12) Jia, Y.; Kerner, R. A.; Grede, A. J.; Rand, B. P.; Giebink, N. C. Continuous-wave lasing in an organic−inorganic lead halide perovskite semiconductor. *Nat. Photonics* **2017**, *11* (12), 784.

(13) Wang, N.; Cheng, L.; Ge, R.; Zhang, S.; Miao, Y.; Zou, W.; Yi, C.; Sun, Y.; Cao, Y.; Yang, R. Perovskite light-emitting diodes based on solution-processed self-organized multiple quantum wells. *Nat. Photonics* **2016**, *10* (11), 699.

(14) Gélvez-Rueda, M. C.; Hutter, E. M.; Cao, D. H.; Renaud, N.; Stoumpos, C. C.; Hupp, J. T.; Savenije, T. J.; Kanatzidis, M. G.; Grozema, F. C. Interconversion between free charges and bound excitons in 2D hybrid lead halide perovskites. *J. Phys. Chem. C* **2017**, *121* (47), 26566.

DOI: 10.1021/acscentsci.9b00839
ACS Cent. Sci. 2019, 5, 1857−1865

(15) Straus, D. B.; Kagan, C. R. Electrons, excitons, and phonons in two-dimensional hybrid perovskites: connecting structural, optical, and electronic properties. *J. Phys. Chem. Lett.* **2018**, *9* (6), 1434.
(16) Grancini, G.; Roldán-Carmona, C.; Zimmermann, I.; Mosconi, E.; Lee, X.; Martineau, D.; Narbey, S.; Oswald, F.; De Angelis, F.; Graetzel, M. One-year stable perovskite solar cells by 2D/3D interface engineering. *Nat. Commun.* **2017**, *8*, 15684.
(17) Wang, Z.; Shi, Z.; Li, T.; Chen, Y.; Huang, W. Stability of perovskite solar cells: a prospective on the substitution of the A cation and X anion. *Angew. Chem., Int. Ed.* **2017**, *56* (5), 1190.
(18) Berhe, T. A.; Su, W.-N.; Chen, C.-H.; Pan, C.-J.; Cheng, J.-H.; Chen, H.-M.; Tsai, M.-C.; Chen, L.-Y.; Dubale, A. A.; Hwang, B.-J. Organometal halide perovskite solar cells: degradation and stability. *Energy Environ. Sci.* **2016**, *9* (2), 323.
(19) Zhao, L.; Gao, J.; Lin, Y. L.; Yeh, Y. W.; Lee, K. M.; Yao, N.; Loo, Y. L.; Rand, B. P. Electrical stress influences the efficiency of CH3NH3PbI3 perovskite light emitting devices. *Adv. Mater.* **2017**, *29* (24), 1605317.
(20) Leijtens, T.; Hoke, E. T.; Grancini, G.; Slotcavage, D. J.; Eperon, G. E.; Ball, J. M.; De Bastiani, M.; Bowring, A. R.; Martino, N.; Wojciechowski, K.; McGehee, M. D.; Snaith, H. J.; Petrozza, A. Mapping Electric Field-Induced Switchable Poling and Structural Degradation in Hybrid Lead Halide Perovskite Thin Films. *Adv. Energy Mater.* **2015**, *5* (20), 1500962.
(21) Azpiroz, J. M.; Mosconi, E.; Bisquert, J.; De Angelis, F. Defect migration in methylammonium lead iodide and its role in perovskite solar cell operation. *Energy Environ. Sci.* **2015**, *8* (7), 2118.
(22) Yang, T. Y.; Gregori, G.; Pellet, N.; Grätzel, M.; Maier, J. The significance of ion conduction in a hybrid organic−inorganic lead-iodide-based perovskite photosensitizer. *Angew. Chem., Int. Ed.* **2015**, *54* (27), 7905.
(23) Egger, D. A.; Kronik, L.; Rappe, A. M. Theory of hydrogen migration in organic−inorganic halide perovskites. *Angew. Chem., Int. Ed.* **2015**, *54* (42), 12437.
(24) Eames, C.; Frost, J. M.; Barnes, P. R.; O'regan, B. C.; Walsh, A.; Islam, M. S. Ionic transport in hybrid lead iodide perovskite solar cells. *Nat. Commun.* **2015**, *6*, 7497.
(25) Meloni, S.; Moehl, T.; Tress, W.; Franckevicius, M.; Saliba, M.; Lee, Y. H.; Gao, P.; Nazeeruddin, M. K.; Zakeeruddin, S. M.; Rothlisberger, U.; Graetzel, M. Ionic polarization-induced current−voltage hysteresis in CH 3 NH 3 PbX 3 perovskite solar cells. *Nat. Commun.* **2016**, *7*, 10334.
(26) Tress, W.; Marinova, N.; Moehl, T.; Zakeeruddin, S. M.; Nazeeruddin, M. K.; Grätzel, M. Understanding the rate-dependent J−V hysteresis, slow time component, and aging in CH 3 NH 3 PbI 3 perovskite solar cells: the role of a compensated electric field. *Energy Environ. Sci.* **2015**, *8* (3), 995.
(27) Snaith, H. J.; Abate, A.; Ball, J. M.; Eperon, G. E.; Leijtens, T.; Noel, N. K.; Stranks, S. D.; Wang, J. T.-W.; Wojciechowski, K.; Zhang, W. Anomalous hysteresis in perovskite solar cells. *J. Phys. Chem. Lett.* **2014**, *5* (9), 1511.
(28) Unger, E. L.; Hoke, E. T.; Bailie, C. D.; Nguyen, W. H.; Bowring, A. R.; Heumüller, T.; Christoforo, M. G.; McGehee, M. D. Hysteresis and transient behavior in current−voltage measurements of hybrid-perovskite absorber solar cells. *Energy Environ. Sci.* **2014**, *7* (11), 3690.
(29) O'Regan, B. C.; Barnes, P. R.; Li, X.; Law, C.; Palomares, E.; Marin-Beloqui, J. M. Optoelectronic studies of methylammonium lead iodide perovskite solar cells with mesoporous TiO2: separation of electronic and chemical charge storage, understanding two recombination lifetimes, and the evolution of band offsets during J−V hysteresis. *J. Am. Chem. Soc.* **2015**, *137* (15), 5087.
(30) Homes, C.; Vogt, T.; Shapiro, S.; Wakimoto, S.; Ramirez, A. Optical response of high-dielectric-constant perovskite-related oxide. *Science* **2001**, *293* (5530), 673.
(31) Juarez-Perez, E. J.; Sanchez, R. S.; Badia, L.; Garcia-Belmonte, G.; Kang, Y. S.; Mora-Sero, I.; Bisquert, J. Photoinduced giant dielectric constant in lead halide perovskite solar cells. *J. Phys. Chem. Lett.* **2014**, *5* (13), 2390.
(32) Cho, H.; Jeong, S.-H.; Park, M.-H.; Kim, Y.-H.; Wolf, C.; Lee, C.-L.; Heo, J. H.; Sadhanala, A.; Myoung, N.; Yoo, S.; Im, S. H.; Friend, R. H.; Lee, T.-W. Overcoming the electroluminescence efficiency limitations of perovskite light-emitting diodes. *Science* **2015**, *350* (6265), 1222.
(33) Zhu, H.; Fu, Y.; Meng, F.; Wu, X.; Gong, Z.; Ding, Q.; Gustafsson, M. V.; Trinh, M. T.; Jin, S.; Zhu, X. Lead halide perovskite nanowire lasers with low lasing thresholds and high quality factors. *Nat. Mater.* **2015**, *14* (6), 636.
(34) Wei, H.; Fang, Y.; Mulligan, P.; Chuirazzi, W.; Fang, H.-H.; Wang, C.; Ecker, B. R.; Gao, Y.; Loi, M. A.; Cao, L.; Huang, J. Sensitive X-ray detectors made of methylammonium lead tribromide perovskite single crystals. *Nat. Photonics* **2016**, *10* (5), 333.
(35) Zhao, L.; Tian, H.; Silver, S. H.; Kahn, A.; Ren, T.-L.; Rand, B. P. Ultrasensitive Heterojunctions of Graphene and 2D Perovskites Reveal Spontaneous Iodide Loss. *Joule* **2018**, *2* (10), 2133.
(36) Zhao, Y.-C.; Zhou, W.-K.; Zhou, X.; Liu, K.-H.; Yu, D.-P.; Zhao, Q. Quantification of light-enhanced ionic transport in lead iodide perovskite thin films and its solar cell applications. *Light: Sci. Appl.* **2017**, *6* (5), No. e16243.
(37) Tsai, H.; Asadpour, R.; Blancon, J.-C.; Stoumpos, C. C.; Durand, O.; Strzalka, J. W.; Chen, B.; Verduzco, R.; Ajayan, P. M.; Tretiak, S.; Even, J.; Alam, M. A.; Kanatzidis, M. G.; Nie, W.; Mohite, A. D. Light-induced lattice expansion leads to high-efficiency perovskite solar cells. *Science* **2018**, *360* (6384), 67.
(38) Zhao, L.; Kerner, R. A.; Xiao, Z.; Lin, Y. L.; Lee, K. M.; Schwartz, J.; Rand, B. P. Redox chemistry dominates the degradation and decomposition of metal halide perovskite optoelectronic devices. *ACS Energy Lett.* **2016**, *1* (3), 595.
(39) Kato, Y.; Ono, L. K.; Lee, M. V.; Wang, S.; Raga, S. R.; Qi, Y. Silver iodide formation in methyl ammonium lead iodide perovskite solar cells with silver top electrodes. *Adv. Mater. Interfaces* **2015**, *2* (13), 1500195.
(40) Dou, L.; Wong, A. B.; Yu, Y.; Lai, M.; Kornienko, N.; Eaton, S. W.; Fu, A.; Bischak, C. G.; Ma, J.; Ding, T.; Ginsberg, N. S.; Wang, L.-W.; Alivisatos, A. P.; Yang, P. Atomically thin two-dimensional organic-inorganic hybrid perovskites. *Science* **2015**, *349* (6255), 1518.
(41) Liu, Y.; Xiao, H.; Goddard, W. A., III Two-dimensional halide perovskites: tuning electronic activities of defects. *Nano Lett.* **2016**, *16* (5), 3335.
(42) Castellanos-Gomez, A.; Vicarelli, L.; Prada, E.; Island, J. O; Narasimha-Acharya, K L; Blanter, S. I; Groenendijk, D. J; Buscema, M.; Steele, G. A; Alvarez, J V; Zandbergen, H. W; Palacios, J J; van der Zant, H. S J Isolation and characterization of few-layer black phosphorus. *2D Mater.* **2014**, *1* (2), No. 025001.
(43) Souza Filho, A. G.; Chou, S. G.; Samsonidze, G. G.; Dresselhaus, G.; Dresselhaus, M. S.; An, L.; Liu, J.; Swan, A. K.; Unlu, M. S.; Goldberg, B. B.; Jorio, A.; Gruneis, A.; Saito, R. Stokes and anti-Stokes Raman spectra of small-diameter isolated carbon nanotubes. *Phys. Rev. B: Condens. Matter Mater. Phys.* **2004**, *69* (11), 115428.
(44) Jorio, A.; Saito, R.; Hafner, J.; Lieber, C.; Hunter, D.; McClure, T.; Dresselhaus, G.; Dresselhaus, M. Structural (n, m) determination of isolated single-wall carbon nanotubes by resonant Raman scattering. *Phys. Rev. Lett.* **2001**, *86* (6), 1118.
(45) Sze, S. M.; Ng, K. K. *Physics of Semiconductor Devices*; John Wiley & Sons, 2006.
(46) Ghosh, S.; Bachilo, S. M.; Simonette, R. A.; Beckingham, K. M.; Weisman, R. B. Oxygen doping modifies near-infrared band gaps in fluorescent single-walled carbon nanotubes. *Science* **2010**, *330* (6011), 1656.
(47) Zhong, D.; Zhang, Z.; Ding, L.; Han, J.; Xiao, M.; Si, J.; Xu, L.; Qiu, C.; Peng, L.-M. Gigahertz integrated circuits based on carbon nanotube films. *Nature Electron.* **2018**, *1* (1), 40.
(48) Kim, W.; Javey, A.; Vermesh, O.; Wang, Q.; Li, Y.; Dai, H. Hysteresis caused by water molecules in carbon nanotube field-effect transistors. *Nano Lett.* **2003**, *3* (2), 193.

DOI: 10.1021/acscentsci.9b00839
ACS Cent. Sci. 2019, 5, 1857−1865

(49) Henkelman, G.; Uberuaga, B. P.; Jónsson, H. A climbing image nudged elastic band method for finding saddle points and minimum energy paths. *J. Chem. Phys.* **2000**, *113* (22), 9901.
(50) Lin, Q.; Armin, A.; Nagiri, R. C. R.; Burn, P. L.; Meredith, P. Electro-optics of perovskite solar cells. *Nat. Photonics* **2015**, *9* (2), 106.
(51) Gebbie, M. A.; Dobbs, H. A.; Valtiner, M.; Israelachvili, J. N. Long-range electrostatic screening in ionic liquids. *Proc. Natl. Acad. Sci. U. S. A.* **2015**, *112* (24), 7432.
(52) Jia, W.; Cao, Z.; Wang, L.; Fu, J.; Chi, X.; Gao, W.; Wang, L.-W. The analysis of a plane wave pseudopotential density functional theory code on a GPU machine. *Comput. Phys. Commun.* **2013**, *184* (1), 9.
(53) Jia, W.; Fu, J.; Cao, Z.; Wang, L.; Chi, X.; Gao, W.; Wang, L.-W. Fast plane wave density functional theory molecular dynamics calculations on multi-GPU machines. *J. Comput. Phys.* **2013**, *251*, 102.
(54) Hamann, D. Optimized norm-conserving Vanderbilt pseudopotentials. *Phys. Rev. B: Condens. Matter Mater. Phys.* **2013**, *88* (8), No. 085117.
(55) Perdew, J. P.; Burke, K.; Ernzerhof, M. Generalized gradient approximation made simple. *Phys. Rev. Lett.* **1996**, *77* (18), 3865.

DOI: 10.1021/acscentsci.9b00839
ACS Cent. Sci. 2019, 5, 1857−1865